

# Inhomogeneities in single-crystal components

U. Paul and P. R. Sahm

Gießerei-Institut Aachen, Intzestraße 5, 52056 Aachen (Germany)

D. Goldschmidt

Motoren- und Turbinen-Union München G.m.b.H., Dachauer Straße 665, 80995 München (Germany)

## Abstract

The temperature distribution during single-crystal solidification of the Ni-based superalloys SRR99 and CMSX-6 by the Bridgman process was measured at various withdrawal rates in dummy turbine blades. Asymmetric heat flux and cross-section transients influence the geometrical formation of the liquidus isotherm and consequently of dendritic growth. The probability of the formation of structural inhomogeneities such as microporosity, zebras, mosaic structures, etc. is largely dependent on the curvature of the solidification front, which in turn depends on the geometrical arrangement of the ceramic cluster and on the withdrawal rate. The proneness to recrystallization during  $\gamma'$  solutioning at cross-section transients due to casting-induced deformation and misaligned dendrites was also examined. Recrystallization remains confined to highly deformed areas as long as microscopic inhomogeneities acting as obstacles are present during heat treatment. High cycle fatigue tests showed that defects such as porosity and local recrystallization reduce the fatigue strength to about half the fatigue strength of the defect-free materials.

## 1. Introduction

Single-crystal components such as blades and vanes for gas turbines are mostly cast in Bridgman-type furnaces using large moulds usually consisting of many parts [1]. Their geometry is characterized by abrupt variations in their cross-section (inner–outer shroud, core configuration, root–airfoil transition). Therefore high temperature gradients and axisymmetric heat flux at the solidification front established under laboratory conditions cannot be maintained. Gradients are lowered and the heat flux becomes asymmetric. This often results in locally different primary dendrite spacings, extensive porosity clusters where interdendritic feeding is hindered [2, 3] or in recrystallization during  $\gamma'$  solutioning heat treatment due to casting-induced deformations and internal stress [4]. Blade and vane design is dictated by the functions of the components. That is why modifying the blade design in order to meet casting requirements often results in lower performance of gas turbines. Therefore it is essential to optimize the casting process with the objective of avoiding structural inhomogeneities or of relocating them into regions of lower stress. This demands a comprehensive understanding of the mechanisms leading to the formation of these inhomogeneities and methods of overcoming them as well as

the knowledge of their influence on mechanical properties. Some results of a detailed study contributing to this subject will be presented here.

## 2. Experimental procedure

### 2.1. Solidification experiments

Two different specimen types (dummies) representing typical turbine blade cross-section transitions were designed to investigate their influence on the single-crystal dendritic growth in the presence of asymmetric heat flux. Ceramic moulds with four of these dummies arranged around a central runner were manufactured by the investment process. The Ni-based superalloys SRR99 and CMSX-6 were solidified as single crystals in a Bridgman furnace at various withdrawal rates ( $1\text{--}10\text{ mm min}^{-1}$ ). Small thermocouples placed at closely defined positions in the platform region were used to measure the temperature distribution and to calculate the curvature of the liquidus isotherm during the passage of the solidification front. Microstructural characteristics such as dendritic alignment, microporosity and recrystallized grains were correlated with the local solidification conditions. The results were verified by single-crystal solidification experiments with actual turbine blades.

## 2.2. Heat treatment experiments

CMSX-6 specimens containing local surface deformations were heat treated at various temperatures to investigate the influence of the  $\gamma'$  solutioning on recrystallization. The amount of recrystallization was determined by metallographic analysis and correlated to the microstructure produced during heat treatment.

## 2.3. Mechanical testing

High cycle fatigue (HCF) tests were carried out at 850 °C with specially prepared specimens (CMSX-6). These nearly net-shaped specimens were characterized by locally excessive porosity clusters or well-defined recrystallized areas produced by local deformation prior to heat treatment.

## 3. Results

### 3.1. Single-crystal growth at cross-section transients

The root-to-platform transition in turbine blades is critical for single-crystal growth. The position and curvature of the liquidus isotherm depend strongly on the withdrawal rate [5] as well as on the blockage of heat radiation by the platform and cluster in this zone. Excessive ceramic accumulations in the transient region also influence the heat transfer. The position of the solidification front relative to the heater bottom shifts from higher regions down to the baffle with an increase in the withdrawal rate. This results in a change in the overall curvature of the front from convex to concave owing to altered heat radiation conditions. The alignment of the specimen in the mould assembly—regions facing the central runner (inner section) and regions facing the graphite heater (outer section)—causes locally different formations of the liquidus isotherm (Fig. 1). The isotherm is slightly concave in the inner section and convex in the outer section at slow withdrawal rates (1–2 mm min<sup>-1</sup>). Both inner and outer regions show a concave curvature of the isotherm at higher withdrawal rates (5–10 mm min<sup>-1</sup>). If the curvature is concave, the temperature at the platform edge falls below the liquidus temperature during cooling, without dendrite tips from the centre part growing into this region. Either heterogeneous nucleation occurs or the melt is undercooled until the solidification front has advanced far enough for dendrites to grow towards the platform edge. In the ceramic shell system applied, both superalloys SRR99 and CMSX-6 were undercoolable to 17 and 27 K respectively. Therefore a slight undercooling does not automatically cause the loss of the single-crystal structure in the outer platform regions. If the melt is undercooled, the local temperature gradient changes its direction (thermally undercooled melt), which results in a rapid lateral

growth of secondary dendrites towards the edge of the platform (Fig. 2). Lateral growth rates of 30–120 mm min<sup>-1</sup> have been measured depending on the degree of undercooling (2–20 K). The amount of latent heat suddenly released during this fast-growing period can result in recalescence effects in the undercooled platform region. Consequently, local solidification conditions change during dendritic growth, causing locally different primary dendrite spacings in the platform region (Fig. 3). In addition, unidirectional heat transfer is interrupted temporarily. This can result in the partial remelting of small dendrite arms, zebra formation [6] or heterogeneous nucleation in the remaining interdendritic melt.

Furthermore, the local change in growth direction and growing speed in the root-to-platform transition leads to distortions (Fig. 4) of the single-crystal lattice (mosaic structure), increasing the risk of recrystallization in components during heat treatment.

The curvature of the solidification front also affects the formation of micropores in interdendritic regions. At low withdrawal rates ( $v < 2$  mm min<sup>-1</sup>) excessive open porosity caused by a convex curvature of the liquidus isotherm arises in the upper region of the platform facing the heater. Conventional gravity mass feeding is blocked and interdendritic feeding is impeded [6]. A low metallostatic pressure caused by the melt intensifies this effect. Sufficient mass and interdendritic feeding to avoid open porosity is provided by a concave curvature (Fig. 5). However, one has to take into account that a concave liquidus isotherm increases the risk of undercooling and therefore of heterogeneous nucleation.

Another problem is the impeded shrinkage of the metal during cooling caused by a stiff ceramic mould. This results in plastic deformation of the component especially at cross-section transitions. Local plastic deformation can lead to undesired recrystallization during heat treatment.

### 3.2. Recrystallization during $\gamma'$ solutioning

Heating the CMSX-6 specimens with local plastic deformation to just below the  $\gamma'$  solvus leads to the nucleation of a fine layer of recrystallized grains (Fig. 6(a)). When  $\gamma'$  is brought into solution at a higher temperature, some of the very small grains grow into the undeformed part of the specimen. Migrating grain boundaries can be pinned down by microstructural inhomogeneities such as residual eutectics or pores (Fig. 6(b)). However, recrystallization extends over the whole cross-section of the specimen when all the  $\gamma$ - $\gamma'$  eutectic is brought to solution (Fig. 6(c)). Incipient melting at even higher temperature reduces the growth rate of recrystallization again. Molten areas act as obstacles to grain boundary migration. Figure 7

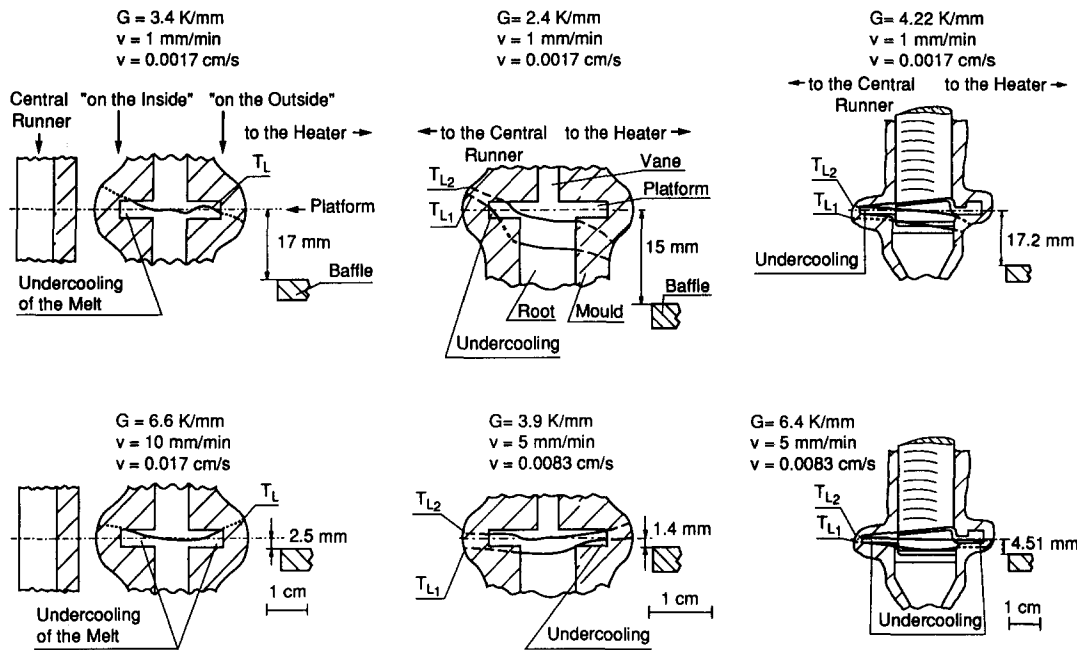


Fig. 1. Position and curvature of the liquidus isotherm (SRR99,  $T_L = 1356$  °C) during the passage through the platform of the dummy as well as the actual turbine blade at various withdrawal rates.

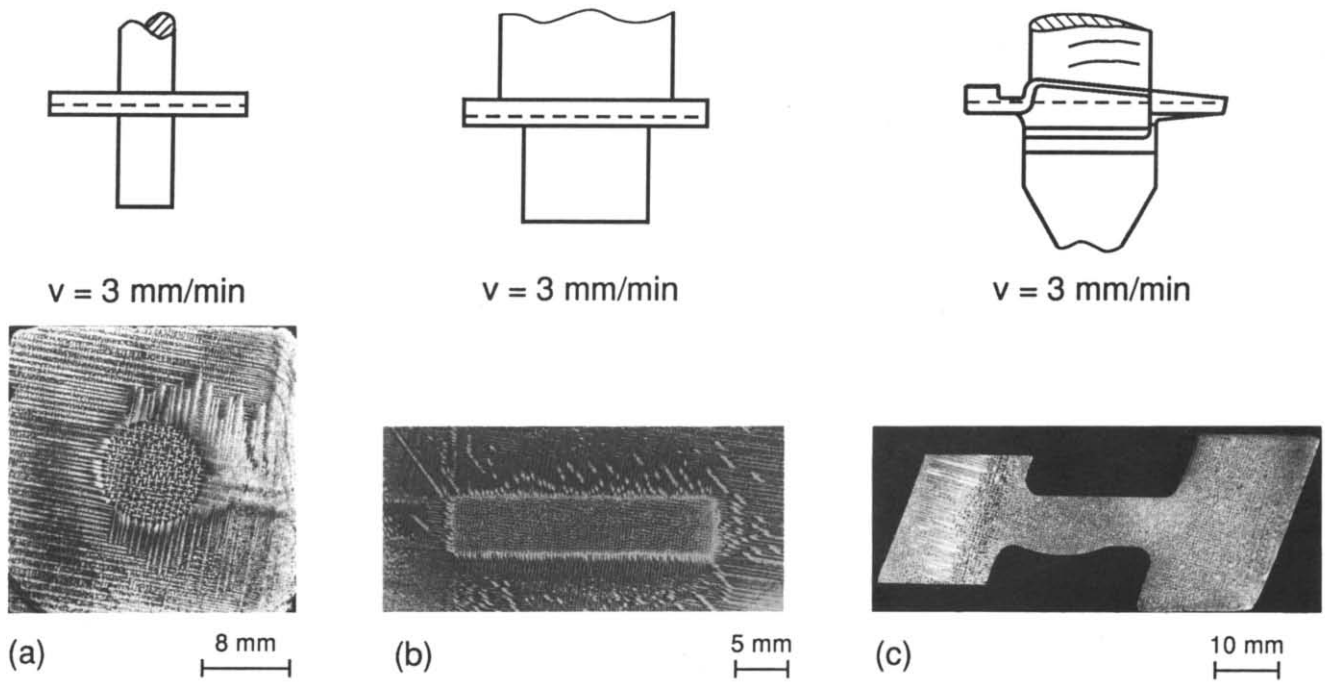


Fig. 2. Dendritic structure in cross-section transitions of (a, b) dummy (CMSX-6) and (c) actual (SRR99) turbine blades characterized by excessive lateral growth ( $30\text{--}120$   $\text{mm min}^{-1}$ ) of secondary dendrites towards outer platform regions (withdrawal rate  $3$   $\text{mm min}^{-1}$ ).

demonstrates the correlations for CMSX-6 specimens surface deformed with a hardness tester prior to heat treatment. The total heat treatment time was 4 h, the heating rate between 1200 °C and the final temperature was  $5$  K  $\text{min}^{-1}$  and the cooling rate was approximately  $150$  K  $\text{min}^{-1}$ .

### 3.3. HCF strength of specimens with porosity clusters or recrystallized grains

The HCF strength of CMSX-6 specimens containing porosity clusters or recrystallized areas of up to 2 mm in diameter is reduced to half the fatigue strength of the defect-free material (Fig. 8). Cracks initiate at the

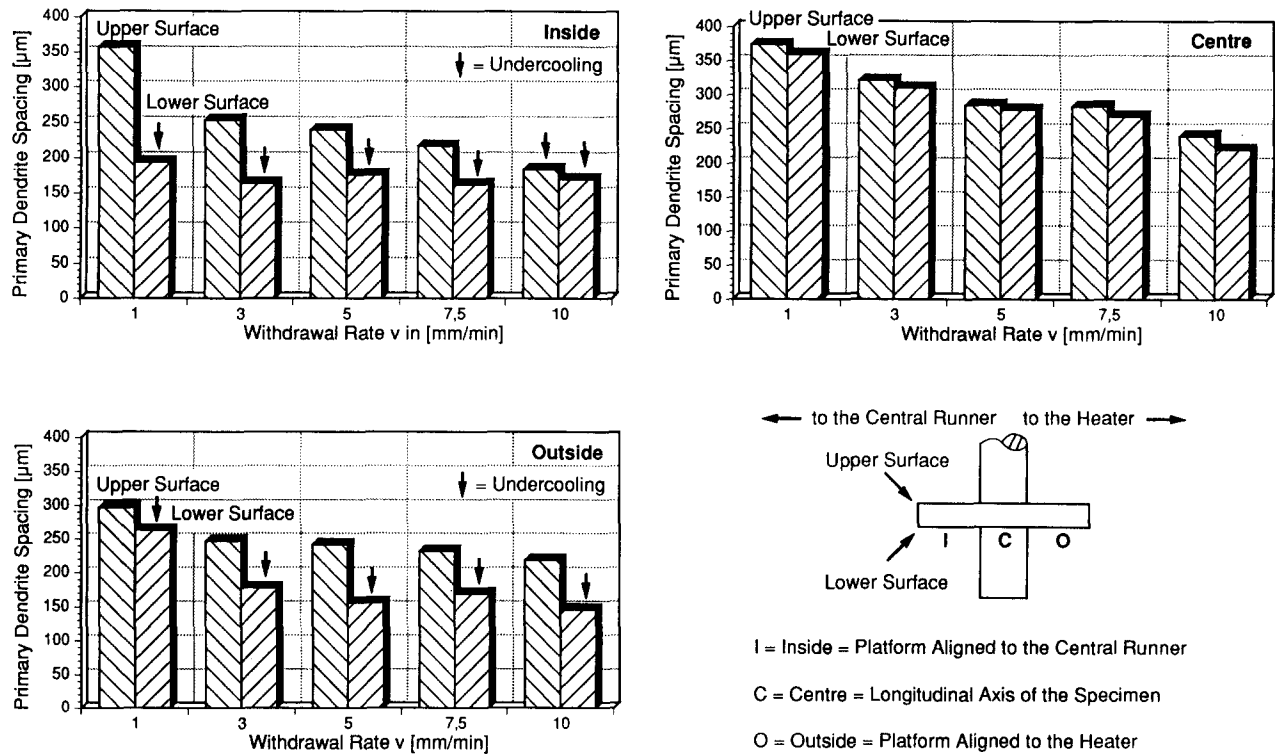


Fig. 3. The locally changing solidification conditions ( $G, R$ ) in the platform result in different dendrite spacings in lateral and vertical directions in this region (SRR99).

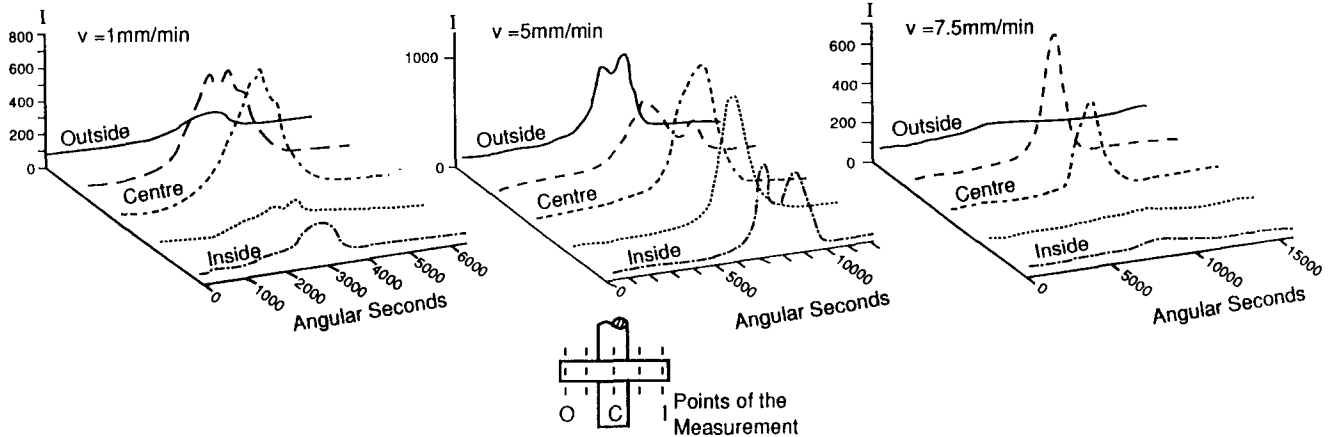


Fig. 4.  $\gamma$ -Diffractometric measurements of crystal distortions in the platform region of a dummy turbine blade at various withdrawal rates (SRR99).

edges of micropores. No dependence on pore size could be ascertained, since the individual pores caused by shrinkage had a length of up to several millimetres. In locally recrystallized specimens cracks initiate at the grain boundary after very few cycles and propagate in a plane perpendicular to the loading direction.

#### 4. Conclusions

The formation of structural inhomogeneities in cross-section transients is caused by the local loss of constant unidirectional growth conditions. The curvature of the liquidus front, which depends on the

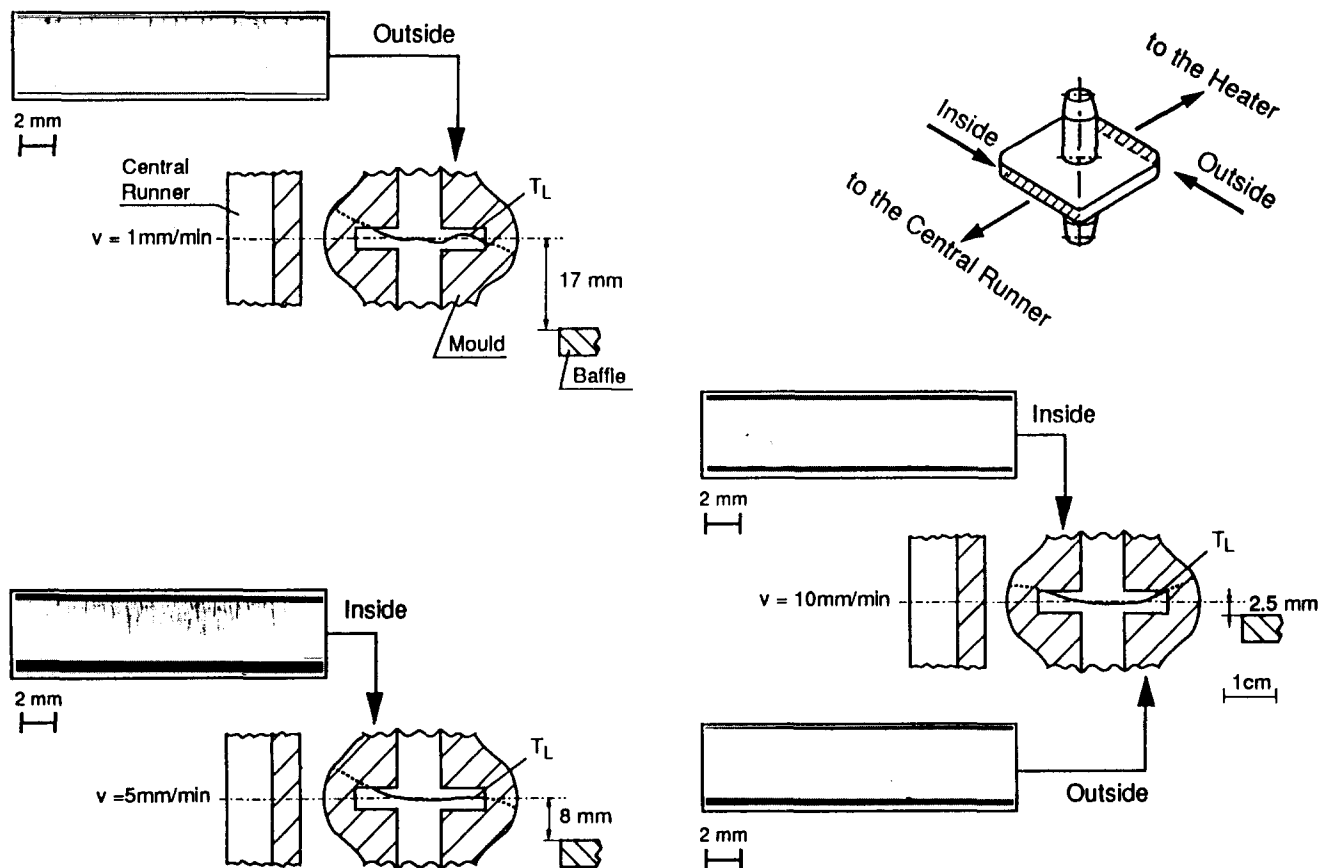


Fig. 5. Micropore formation in the platform region of a dummy turbine blade at various withdrawal rates (SRR99).

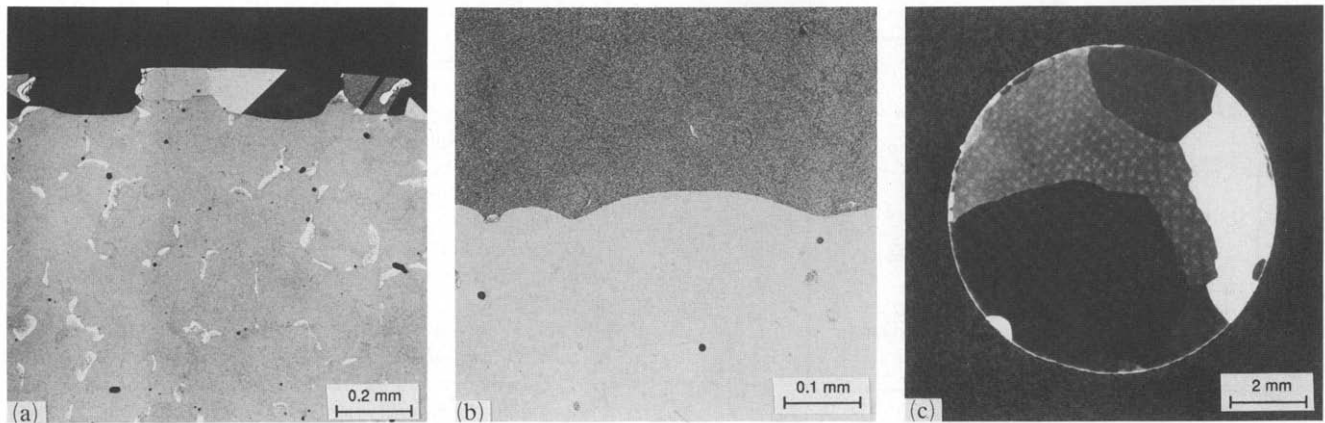


Fig. 6. Recrystallization in surface-deformed CMSX-6 specimens during  $\gamma'$  solutioning: (a) nucleation of a fine layer of recrystallized grains; (b) pinning of migrating grain boundaries by residual eutectic; (c) recrystallization extending over the total specimen cross-section.

location of the front in the mould and on the withdrawal rate, influences the formation of micropores, zebras, misoriented grains and local crystal distortion. Setting feeders or rotating the component longitudi-

nally and/or transversally are ways of avoiding these defects. Recrystallization is influenced mainly by the heat treatment temperature during  $\gamma'$  solutioning. A fully solutioned microstructure gives rise to the excess-

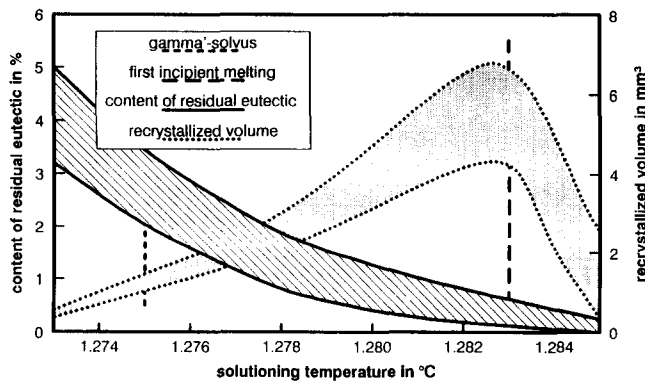


Fig. 7. Recrystallized volume in CMSX-6 specimens locally surface deformed with a hardness tester prior to heat treatment as a function of the solutioning temperature in comparison with residual  $\gamma$ - $\gamma'$  eutectic present after heat treatment (heat treatment time, 4 h; heating rate between 1200 °C and final temperature, 5 K min<sup>-1</sup>; cooling rate from final temperature, 150 K min<sup>-1</sup>).

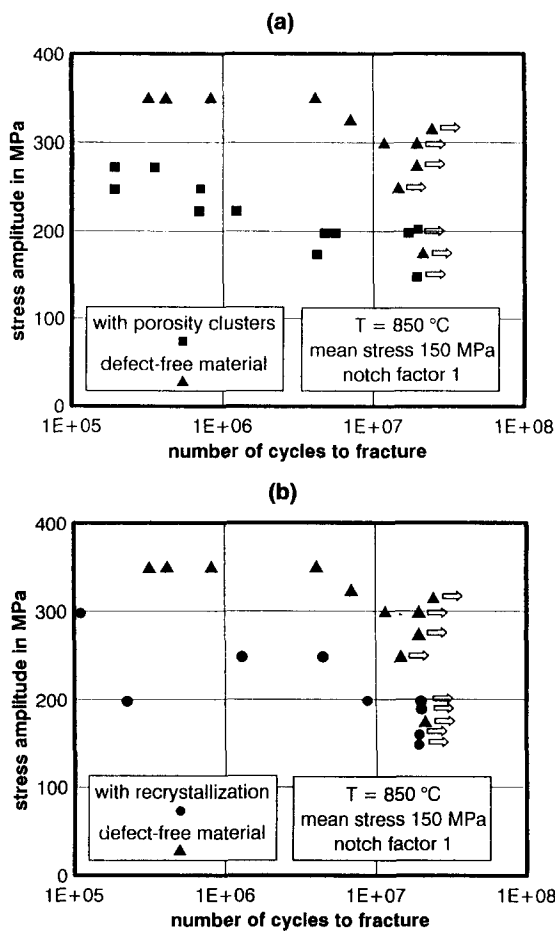


Fig. 8. HCF strength of CMSX-6 specimens containing (a) porosity clusters or (b) recrystallized grains in comparison with defect-free material.

sive growth of small grains which have nucleated in the deformed areas. Porosity clusters and local recrystallization reduce the HCF strength of CMSX-6 to approximately half the strength of defect-free material. However, these defects can be tolerated in blade regions where a lower level of strength is still sufficient.

## References

- 1 M. J. Goulette, P. O. Spilling and R. P. Arthey, in M. Gill, Ch. S. Kortovich, R. H. Brikell, W. B. Kent and J. F. Radavich (eds.), *Proc. 5th Int. Symp. on Superalloys, Seven Springs, October 1984*, Metall. Soc. AIME, Warrendale, PA, 1984, pp. 167-176.
- 2 L. Ouichi, G. Lesoult, G. Lamanthe, R. Hamer, J. M. Theret and E. Bachelet, *Proc. Conf. on High Temperature Alloys for Gas Turbines and Other Applications, Liege, October 1982*, Reidel, Dordrecht, 1982, pp. 955-971.
- 3 J. Lecomte-Beckers, *Proc. 6th Int. Symp. on Superalloys, Seven Springs, September 1988*, Metall. Soc., Warrendale, PA, 1988, pp. 713-721.
- 4 L. G. Fritzemeier, *Proc. 6th Int. Symp. on Superalloys, Seven Springs, September 1988*, Metall. Soc., Warrendale, PA, 1988, pp. 265-274.
- 5 U. Paul, P. R. Sahm, A. Donner, D. Goldschmidt and P. D. Portella, *Proc. 2nd Symp. Materialforschung, Dresden, August 1991*, TUV Rheinland, Köln, 1991, pp. 841-864.
- 6 J. Campbell, *Br. Foundryman*, 62 (1969) 4.